LOng-LIved greenhouse gas PrOducts Performances (LOLIPOP)

WP3100 - Sensitivity of historical climate model simulations to the OLLGHG climatology

D3.2.1 - User Case Study Technical Note

Document Reference	[D3.2.1] LOLIPOP_UCS-PUB_v1.0
Document Authors	Federico Fabiano (CNR-ISAC) Alessandro Montanarini (CNR-ISAC)
Document Approvers	S. Pinnock (ESA, Technical Officer)

Change log:

Version Nr.	Date	Status	Reason for change
Version 1.0	15-11-2025	First submission of the document	N/A

Table of Contents

1 Introduction

The increase in greenhouse gas (GHG) concentrations since 1750 has been primarily driven by human activities, with significant implications for climate change. While carbon dioxide (CO_2) and methane (CH_4) are the dominant drivers, other minor GHGs, such as nitrous oxide (N_2O) and halogenated gases, are also contributing substantially to global warming. In 2019, N_2O levels reached 332 ppb, reflecting a 23% increase similar to natural changes observed over the past 800,000 years (IPCC, 2021). Agriculture is responsible for approximately 60% of atmospheric N_2O, which plays a crucial role in both ozone depletion in the stratosphere and the production of tropospheric ozone. With a global warming potential (GWP) 298 times that of CO_2, N_2O is a potent GHG with a long atmospheric lifetime, making it a significant climate driver (Hassan et al., 2022). N_2O and the halogenated gases (CFCs, HCFCs, ...) contribute significantly to the present-day Radiative Forcing (RF), accounting for about 0.4 W/m^2 altogether, almost 20% of the RF due to CO_2 alone (Forster et al., 2021).

LOLIPOP URD (D1.1) examined the use of "Other" Long-lived Greenhouse Gases (OLLGHGs, i.e. N_2O and other minor GHGs) data in climate modelling, focusing on their global warming potential and their role in the computation of radiative fluxes. The Coupled Model Intercomparison Project (CMIP), particularly Phase 6 (CMIP6, Eyring et al., 2016), represents the largest effort in climate modelling, contributing to the Intergovernmental Panel on Climate Change (IPCC) reports. CMIP6 includes several experiments, such as idealised experiments, historical atmosphere-only and coupled atmosphere-ocean simulations with observed GHG concentrations, and future projections based on different Shared Socio-economic Pathways defining future GHG emissions (SSPs, O'Neill et al., 2016).

The GHG datasets used for these experiments are presented in Meinshausen et al. (2017), which aggregated observational data from surface stations networks like NOAA and AGAGE to estimate global mean concentrations and latitudinal/seasonal variations for each gas. For N_2O, a combination of AGAGE and NOAA/ESRL data is used, with earlier periods reconstructed using Law Dome ice core data. A key challenge is that models require not only surface concentrations but also vertical distributions of gases, which are typically not available from surface measurements alone. To address this, climate models can follow two different strategies:

- models that include a chemistry module (chemistry-climate models) are usually run through emissions directly rather than concentrations and natively simulate the vertical/latitudinal distribution of gases;
- models without a chemistry module (the majority in CMIP6) assume a fixed latitude/height distribution for each GHG, which is then scaled using the observed/projected surface concentrations to account for time evolution;

For the second class of models, a simplified 3-D distribution method for N_2O and CFC-12 is proposed by Meinshausen et al. (2017), assuming a well-mixed troposphere and a latitudinally varying tropopause height.

This case study aims to investigate the impact of the uncertainty in the vertically-resolved climatological distribution of N_2O and minor greenhouse gases on the simulated climate and future projections of a specific climate model, EC-Earth3 (Döscher et al., 2022), described in Section 2.1. The analysis will proceed along the following steps:

- investigate how are N_2O and minor GHGs implemented inside the climate model;
- compare the climatologies currently used as input to the model with other simulated and/or observed climatologies (when available, observational datasets from Task 2200/2300 will be used);
- implement a new/perturbed climatology inside the climate model;
- perform atmosphere-only present-day simulations to study the impact of the new/perturbed climatologies on the radiative fluxes and atmospheric temperature;

This analysis will focus on N_2O alone since - among minor GHGs - it is expected to have the largest effects on the simulated climate.

2 Methods

This section presents the EC-Earth3 model, the assessment regarding the implementation of minor GHGs inside it and updates to the model code necessary for the experimental part of the case study.

2.1 Model description

EC-Earth3 is a state-of-the-art Earth system model, developed by a consortium of European research institutions (Döscher et al., 2022), which includes robust and validated components for the atmosphere (the ECMWF IFS model cy36r4), the ocean (NEMO 3.6; Madec et al., 2017), the sea ice (LIM3; Fichefet and Maqueda, 1997), and land processes (H-Tessel; Balsamo et al., 2009). It is worth noting that v3.3.3 is the same version used for the Coupled Model Intercomparison Project - Phase 6 (CMIP6). The model has been used in the standard CMIP6 resolution TL255L91-ORCA1L75, corresponding to a horizontal resolution of approximately 80 and 100 km in the atmosphere and the ocean, respectively. In the vertical, the atmosphere uses 91 levels (up to 1 hPa) and the ocean 75 levels.

2.1.1 Changes to the model code

In the original version, climatologies are hard-coded and can be modified only by re-compiling the code every time. The model code has been modified to take in input a custom climatology for the relevant gases, without the need for recompiling the code for each new climatology. The code also now accepts input climatology in netCDF format, which can be provided for any of the GHG gases.

2.2 Input data description

2.2.1 Assessment of the implementation of minor GHGs in EC-Earth3 (IFS)

In the Atmosphere-Ocean General Circulation Model (AOGCM) version of EC-Earth3, only the main radiatively-active chemical species are considered, namely: CO_2, CH_4, O_3, N_2O and CFC-12. All minor GHGs are included in an aggregate equivalent species CFC-11-eq, as defined in Meinshausen et al. (2017). The abundance of the various species making up CFC-11-eq is weighted for their absorbance.

For each gas, a latitude/height climatology is implemented in the model, which is then scaled following the time evolution of the global mean surface abundance (following observations for the historical period or scenarios for the future). In the current version of EC-Earth3, the climatologies are hard-coded in the model code. An exception is O_3, which is taken in input from an external netCDF file as a 3D latitude/longitude/height scenario.

The climatology currently implemented for N_2O is assessed. For both gases, the latitude/height distribution is taken from the MOBIDIC chemistry model (Cariolle and Brard, 1984; Cariolle et al., 2007).

The climatology of N_2O and CFC-11 has been retrieved from the model code and compared to:

1. the simple parametrization in Meinshausen et al., 2017 (Mein17);
2. climatologies extracted from a state-of-the-art chemistry-climate model: CESM-WACCM AerChemMIP historical simulation during 1990-2014 (WACCM);

In Figure 1, we present a comparison of the N_2O climatology across different models and datasets. The left panel shows the N_2O climatology currently implemented in the EC-Earth3 climate model. The middle panels display two alternative N_2O climatologies: the top panel shows the Meinshausen et al. (2017) (Mein17) climatology and the bottom panel presents the WACCM climatology. The right panels illustrate the differences between the Mein17 (top) and WACCM (bottom) climatologies, compared to the current EC-Earth3 N_2O implementation. Panels on the right highlight the spatial and temporal variations in N_2O concentrations between the different climatologies, providing insight into the potential impacts of using different N_2O input data in climate models. In both cases, significant

differences are seen in the lower stratosphere, peaking between 20 and 40 km depending on latitude, and extending up to the upper mesosphere. Differences are more evident and appear at lower altitudes at the poles, where the signal is expected to be more evident. Both alternative datasets considered also agree in showing that the current EC-Earth3 implementation is probably over-estimating the N_2O concentration in the stratosphere and mesosphere.

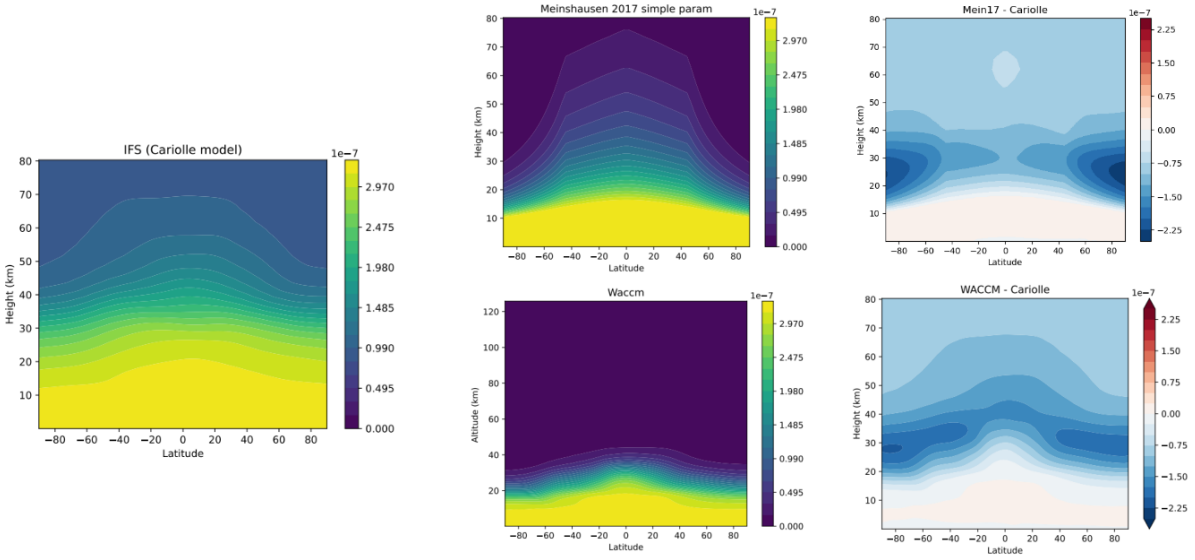

Figure 1. Left panel: N2O climatology currently implemented in EC-Earth3. Middle panels: Mein17 (top) and WACCM (bottom) climatologies. Right panels: difference between Mein17 (top) and WACCM (bottom) climatologies and the current EC-Earth3 implementation.

The WACCM climatology is preferred for the first sensitivity test presented in Section 3, as it is produced through a full-physics chemistry-climate model and is expected to better represent seasonal and latitudinal variations with respect to the simple parametrization in Meinshausen et al. (2017).

2.2.2 N_2O climatologies from LOLIPOP limb satellite measurements

Now we move the focus to the real data with the climatologies of the N_2O concentrations obtained from the limb satellite products prepared by WP2000. Available data are from ACE-FTS (Bernath et al., 2005), MIPAS (Fischer et al., 2008), MLS (Waters et al., 1999; Barath et al., 1993), ODIN (Frisk et al., 2003). The time and latitudinal coverage of the four instruments varies and none of them covers the whole region and seasonal variability needed as input to the model, so an extrapolation/filling of the

datasets is needed before using them as input climatologies. Figure 2 shows the time- and zonal-average N_2O mixing ratio for the four instruments (ACE-FTS: 2004-2024, MIPAS: 2002-2012, MLS: 2004-2024, ODIN: 2002-2024).

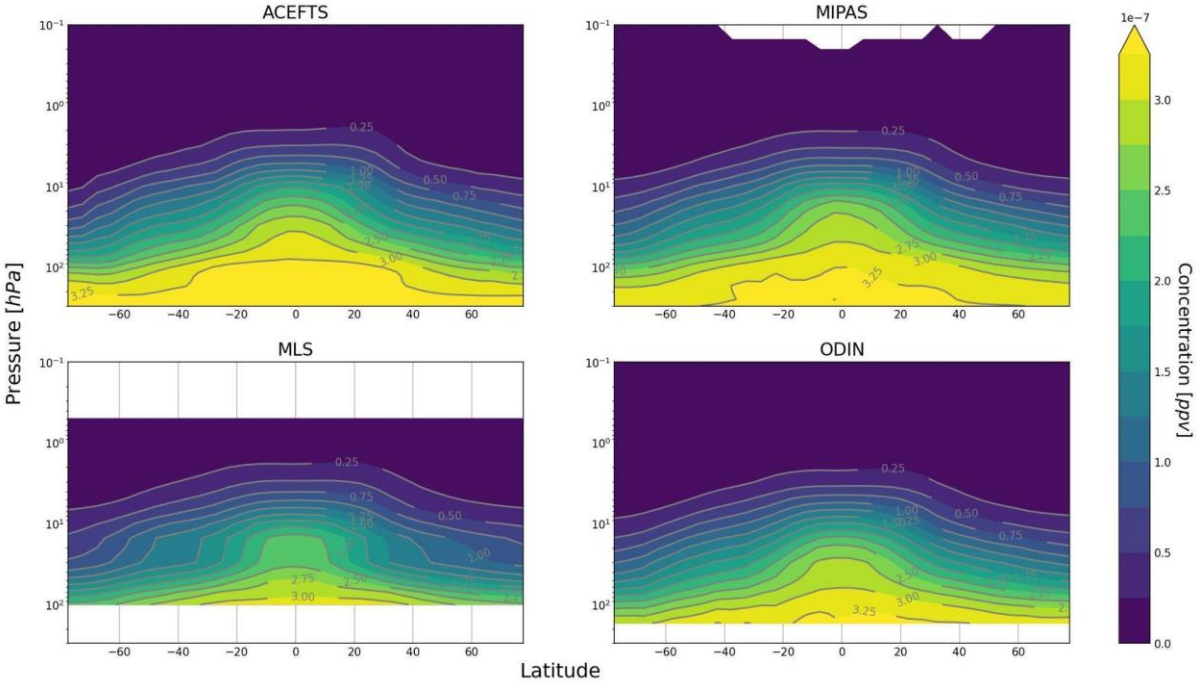

Figure 2. Time- and zonal-average N_2O volume mixing ratio for the four satellite instruments.

Figure 3 shows the difference of each instruments' climatology with respect to the WACCM model climatology described in the previous section. Apart from MLS, where the difference reaches 20% of the absolute value in the lower stratosphere, differences with WACCM are generally of the order of 10 ppb. Moreover, part of the difference might be due to the different periods considered for each instrument and to the different latitudinal and seasonal coverage.

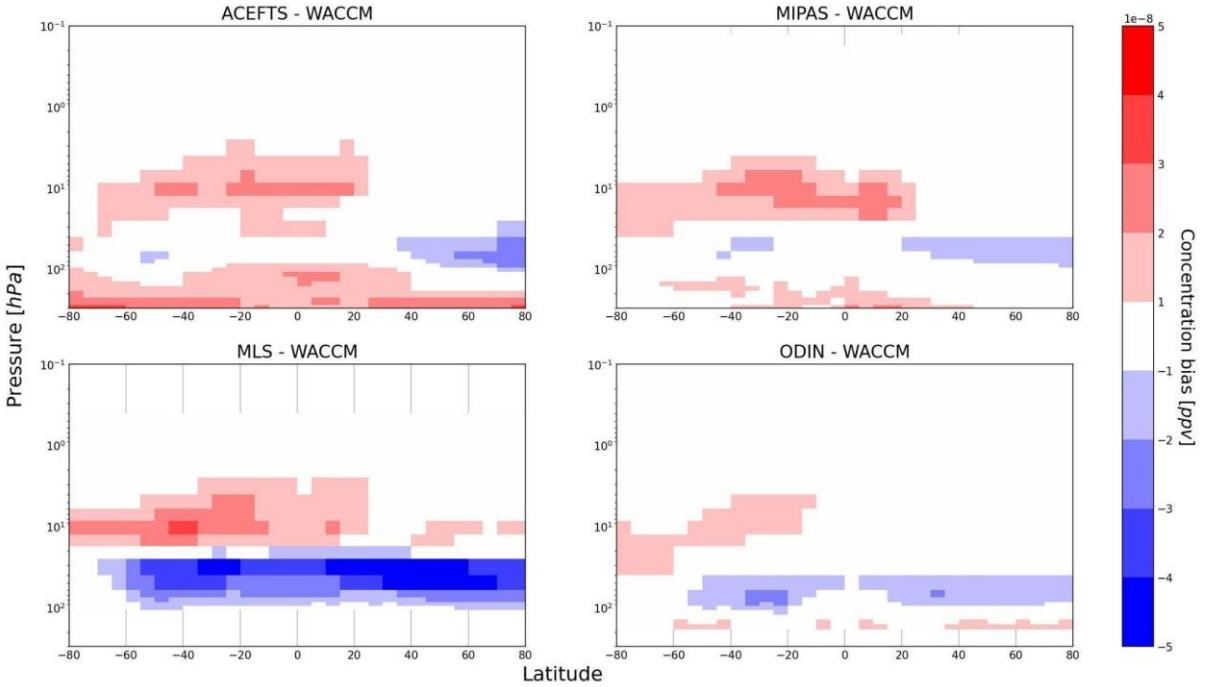

Figure 3. Satellite instruments' time- and zonal-average N_2O volume mixing ratio difference with respect to CESM-WACCM climatology.

Indeed, when looking at the monthly climatologies, the situation is more complicated. In particular, the ACE-FTS dataset, which is the one reaching the highest altitude, shows systematic missing values for many latitudinal bands in various months (not shown), thus not allowing to reconstruct the seasonal variations and possibly biasing the annual average.

Figure 4 (left panel) shows the time- and global-mean VMR profile of N_2O from the various datasets, compared to the original input to the EC-Earth3 model (orig) and to the WACCM climatology. The right panel of Figure 4 shows the quality of the global mean, measured as the fraction of data points containing a value. As can be seen, despite being the only dataset to reach 0.01 hPa, less than half of data points (month, latitude, height) are defined for ACE-FTS.

Among the other datasets, MIPAS and MLS show the best coverage in the critical region between 100 and 1 hPa. However, MLS is clearly biased with respect to the other measurements starting from around 50 hPa and above. ODIN is in good agreement with MIPAS but has generally less data points defined. Despite the shorter timeseries (2002-2012), the MIPAS dataset appears the most reliable to catch the seasonal and latitudinal variations of the N_2O VMR between 100 and 1 hPa. A more detailed view is provided in Figure 5, which shows the difference of each dataset with respect to WACCM. The bias of MLS is evident from there, as well as the good agreement among the other measurements. The difference at the tropospheric altitudes is attributable to the different period considered for the

instruments and for the WACCM climatology (1979-2014), and accounting for a trend in tropospheric N_2O concentration of about 1 ppb/year (differences are of the order of 10 ppb there).

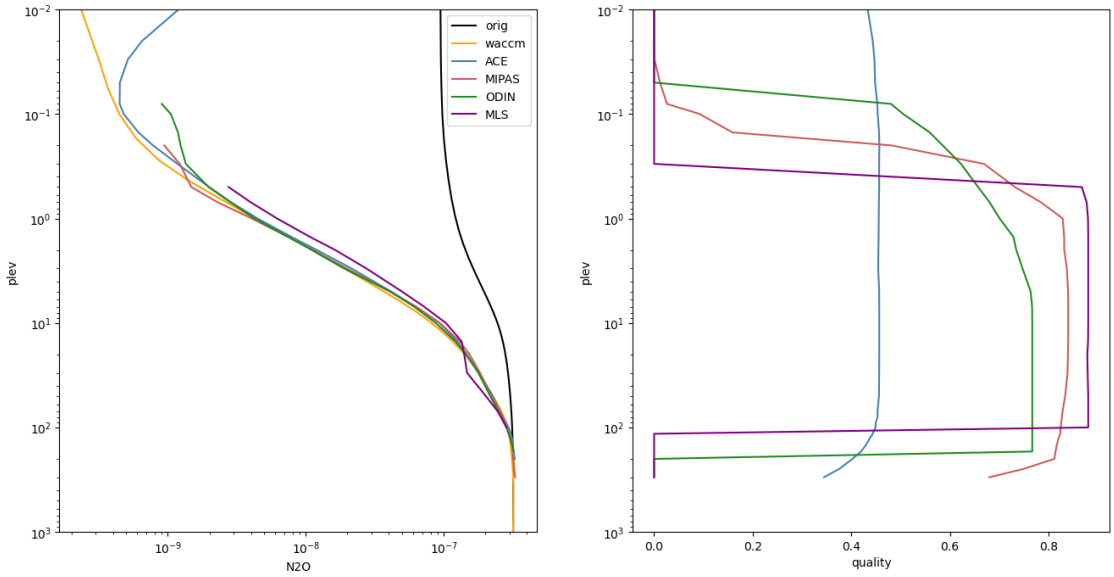

Figure 4. Time- and global-mean N_2O VMR profile from the various datasets, compared to the original climatology in EC-Earth3 (orig) and to the WACCM climatology (left panel). The right panel shows the quality of the global mean, measured as the fraction of points defined (month, latitude, height) when performing the global mean. Only regions where the quality is larger than 0.4 are plotted in the left panel.

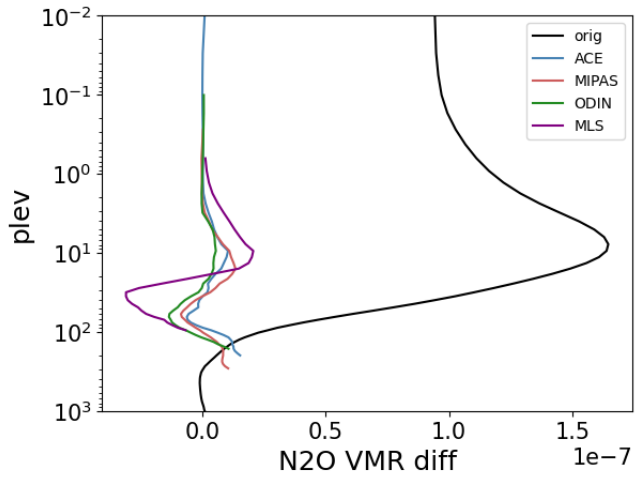

Figure 5. As in Figure 4, left panel, but showing differences with respect to WACCM climatology.

As a further test, the monthly variations with respect to the annual mean are compared now between the MIPAS dataset and WACCM in Figure 6. The visual agreement between the patterns is remarkable, with the main features well reproduced in the simulated field, with only minor details differing (but possibly attributable to other causes, such as the different period considered and interannual variability).

This gives further confidence in the reliability of the WACCM climatology as input to the EC-Earth3 model in Section 3.2.

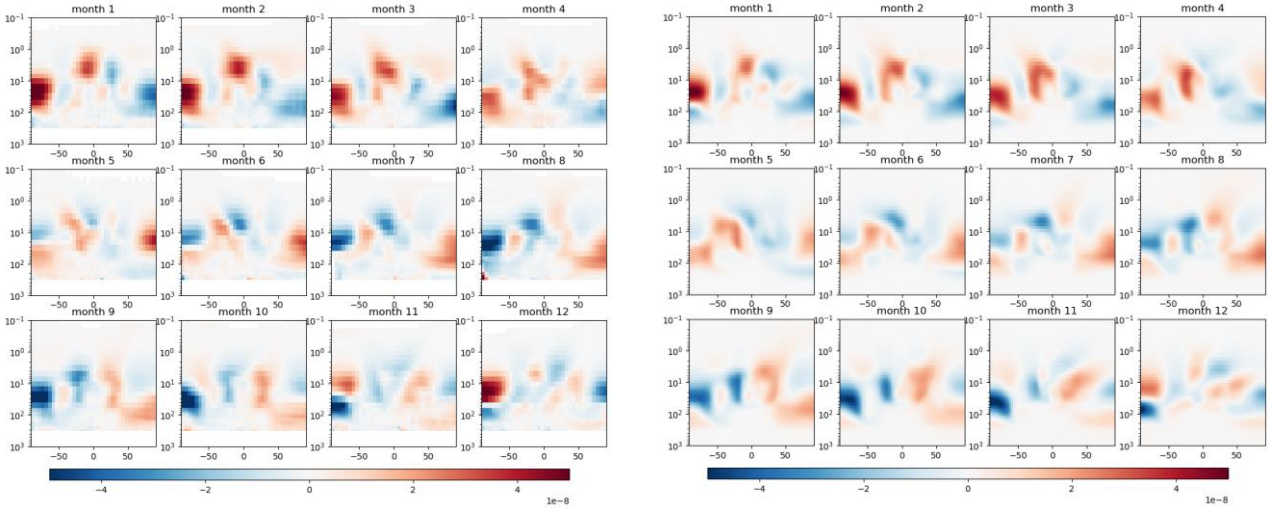

Figure 6. Stamp plot of the seasonal variations in the MIPAS dataset (left) and in the WACCM dataset (right).

3 Results

This Section presents the main results of the case study, regarding:

- an offline estimation of the radiative effects expected with a modified N_2O concentration in the stratosphere and mesosphere;
- the sensitivity simulations performed with EC-Earth3 to assess the impact of using an updated climatology for N_2O.

3.1 Sensitivity of radiative fluxes and local heating rates to stratospheric N_2O concentration

The first question is whether a change in the N_2O concentration in the stratosphere of the order of 100-150 ppb is able to significantly affect the radiative fluxes and, consequently, the heating rates, such as to impact the simulated climate. Of course, since the changes are quite high in the atmosphere, it is quite unlikely that they would impact the surface climate, but they may be strong enough to modify the temperature structure in the middle atmosphere and, possibly, the outgoing longwave radiation.

Aiming at giving a first quantitative answer to this question, an offline radiative transfer calculation is performed using ecRad, a fast radiative transfer model used in more recent versions of the IFS and freely available online (Hogan and Bozzo, 2018).

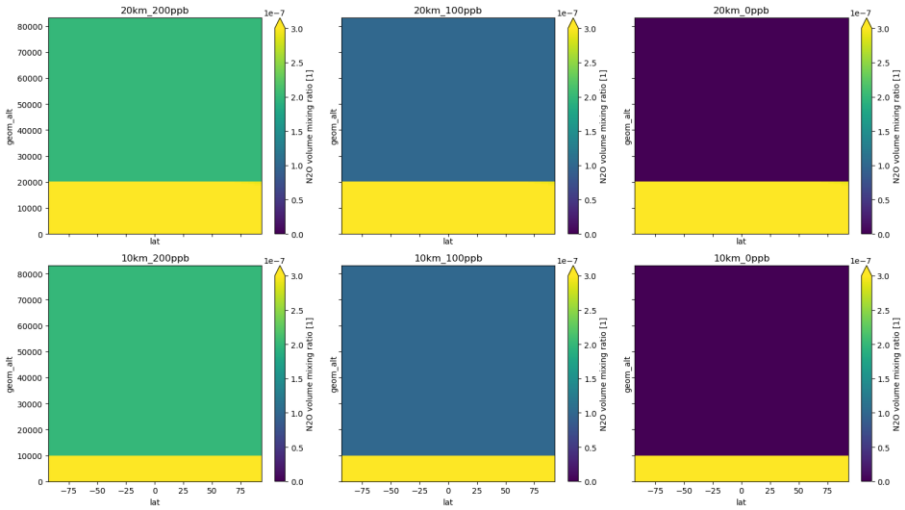

Figure 7. Idealised latitude/height distributions used for the radiative sensitivity assessment.

Figure 7 shows the six idealised latitude/height distributions used for the radiative sensitivity assessment: the original profile is set to a fixed value of 200/100/0 ppb above 20 km (first row) or 10

km (second row). ecRad has been run with each of these concentrations, using as input the test atmosphere provided with the ecRad code (representing a meridional transect on a specific day in a former IFS simulation).

The result of the perturbation on outgoing longwave fluxes is shown in Figure 8.

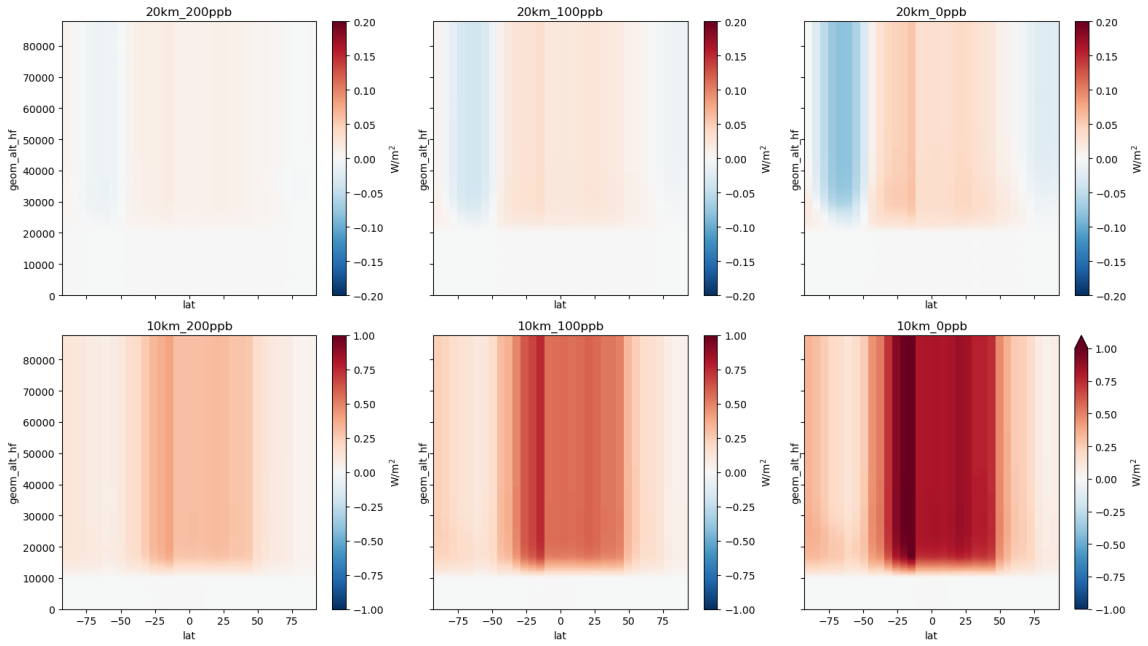

Figure 8. Clear-sky outgoing lowgwave radiation anomalies obtained with the six idealized N2O climatologies shown in Figure 2. Differences with respect to the control calculation with the original N2O profile.

As can be seen from Figure 3, the magnitude of the changes can reach up to 1 W/m^2 for perturbations starting as low as 10 km, and about 0.1 W/m^2 for perturbations starting at 20 km. The "20 km - 100 ppb" case is the closer one to the actual difference between the reference N_2O climatology and the two alternative climatologies explored in Section 2.2.1.

Though small, these changes might be able to affect the local climate. Local heating rates have been calculated as the vertical gradient of the net upward longwave radiation. The resulting heating rate anomalies for the six cases above are shown in Figure 4. The results regarding the local heating rates are promising. As can be seen, the region between 20 and 40 km is apparently sensitive to the perturbation of the N_2O profile, reaching up to 0.2 K/day in specific parts of the atmosphere. The peculiar pattern is explained by the temperature structure of the test atmosphere used (Figure 9, right panel).

In conclusion, the results of the offline sensitivity tests show that a general warming of the stratosphere is to be expected in response to a decrease in the local N_2O concentration (since N_2O

acts as a coolant there), and that the magnitude of the change might be detectable since the heating rates are perturbed up to 0.2 K/day.

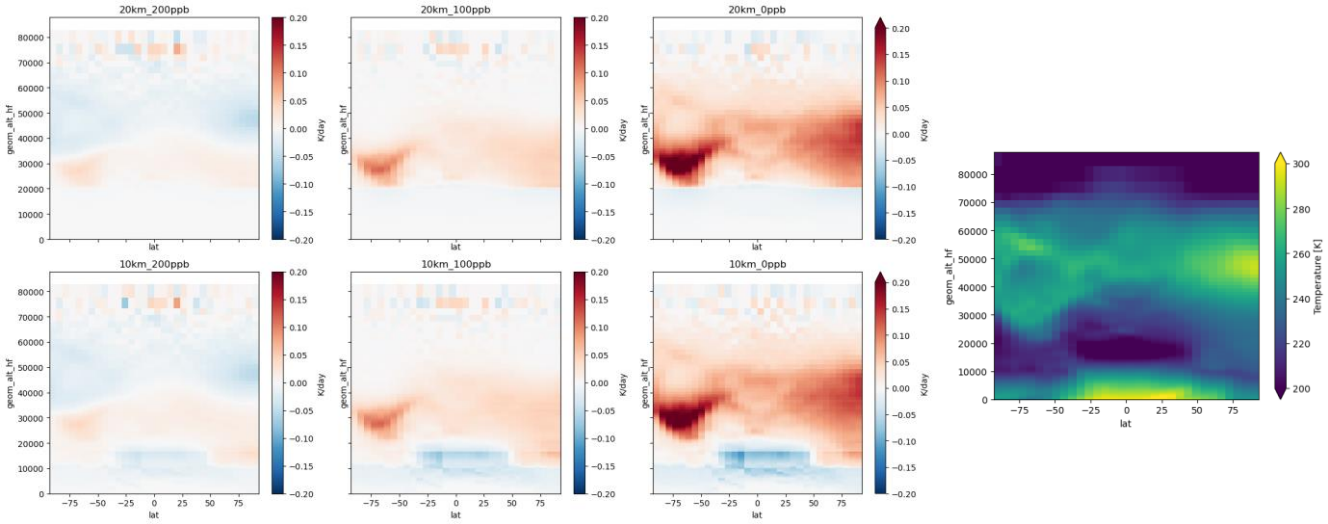

Figure 9. Local heating rate anomalies in K/day obtained with the six idealized N_2O climatologies shown in Figure 7. Differences with respect to the control calculation with the original N_2O profile. Rightmost panel: 3D temperature of the test atmosphere used.

3.2 Sensitivity simulations with EC-Earth3 with modified N_2O climatology

Following the analysis in Section 2.2, a first sensitivity simulation has been run with the EC-Earth3 model. We first briefly describe here the experimental setup and then show the results of the analysis.

3.2.1 Setup of the simulations and preliminary assessment

The simulations have been run in atmosphere-only mode, where the atmosphere is modelled independently, with a one-way interaction with the ocean. This configuration uses observed sea-surface temperatures (SSTs) and sea-ice concentration (SIC), which are derived from the CMIP6 AMIP (Atmospheric Model Intercomparison Project) protocol. These observations represent the actual observed conditions during the simulation period, providing a realistic boundary for the atmospheric model. The time span covers the period from 2000 to 2014, allowing the model to examine atmospheric conditions and radiative forcing over this specific time frame. The choice of the recent period is to allow a better match with available observational data. CMIP6 AMIP SST data end in 2015 but can be extended up to 2024 in future simulations. The simulations incorporate the evolution of global-mean greenhouse gas (GHG) concentrations as outlined in the historical/AMIP CMIP6 protocol.

The experiment consists of two sets of simulations:

- 'control' is the control ensemble, which uses the original N_2O climatology implemented in EC-Earth3;
- 'waccm' is the sensitivity ensemble, which uses the N_2O climatology obtained from the WACCM model;

For each ensemble, 10 AMIP simulations spanning 2000-2014 have been performed, for a total of 150 years each. About 210 thousand core hours were used on a high-performance computing platform to produce the two ensembles (~700 core hours per simulated year).

The ensemble simulations were performed following the preliminary assessment done in Version 0.1 of this technical note, which demonstrated the need to increase the sample size of the simulations to allow disentangle the small effect expected on the radiative fluxes and the temperature profile from internal variability. We report Figure 6 of the preliminary assessment (now Figure 10) to show the difference in the simulated zonal-average temperature profile for the first two simulations of each ensemble.

To better represent the difference in the middle atmosphere, pressure has been used as a vertical coordinate with a logarithmic axis. As can be seen, some regions stand out the noise threshold, highlighting a possible impact of the modified N_2O profile. Interestingly, with the exception of the north polar stratosphere, all the significant regions show a positive anomaly, in line with what

expected from Section 3.1. However, the small extent of the regions standing outside the non-significant threshold and the peculiar pattern, suggest that the signal-to-noise ratio is still too low to call for a clear impact of the modified climatology. This motivated the need to perform an ensemble analysis, which is presented in the next section.

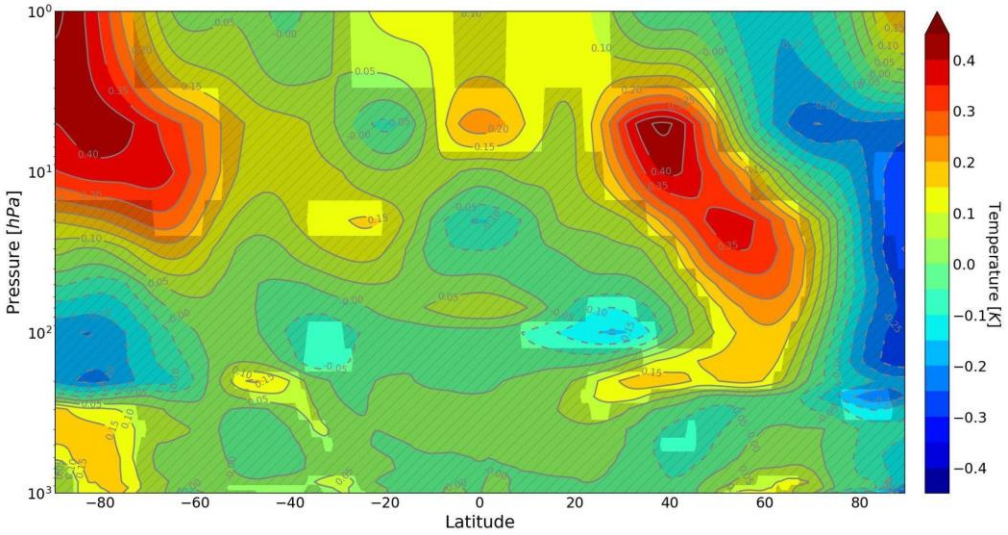

Figure 10. Recalling Figure 6 of the preliminary assessment. Time- and zonal-mean atmospheric temperature, difference between the first member of the waccm and control ensembles. Non-significant regions are masked.

3.2.2 Ensemble analysis

We report here the final results of the sensitivity experiment, based on the two ensembles of simulations. Based on the results obtained through the offline calculations in Section 3.1, the analysis focuses on two fields:

- the radiative fluxes at TOA, which should bring the signature of the modified N_2O profiles;
- the vertical temperature profile, which is expected to be affected in the middle atmosphere since heating rates are modified where the N_2O concentration is changed;

We do not consider surface fluxes since the changes applied are very small and at stratospheric altitudes, hence not expected to significantly influence the tropospheric climate.

Figure 11 shows how each simulation in the WACCM ensemble behaves with respect to the control ensemble mean in the time and zonal-mean atmospheric temperature. On average the simulation members have a warmer stratosphere, and the largest variability is registered at the poles. The North

Pole has greater variability with 3 members performing a high-stratosphere cooling, while the South Pole shows a more coherent warming across all members.

When averaging across the ensemble, the picture is much clearer. Figure 12 shows the main result of the study, which demonstrates the effect of the modified N_2O climatology on the climate model simulation. Non-significant regions have been masked according to two criteria: 1) regions where the absolute difference is smaller than the standard error of the ensemble mean; 2) regions where less than 8 out of 10 members agree on the sign of the change.

A consistent warming signal emerges now in the stratosphere at almost all latitudes, with the only exception of the North pole. The warming is of the order of a tenth of degree, concentrated in the range between 30 and 2 hPa (corresponding roughly to 25-45km), thus between mid-stratosphere to stratopause. The South pole shows an increased signal (up to 0.3 K) and extending further down towards the lower stratosphere and upper troposphere.

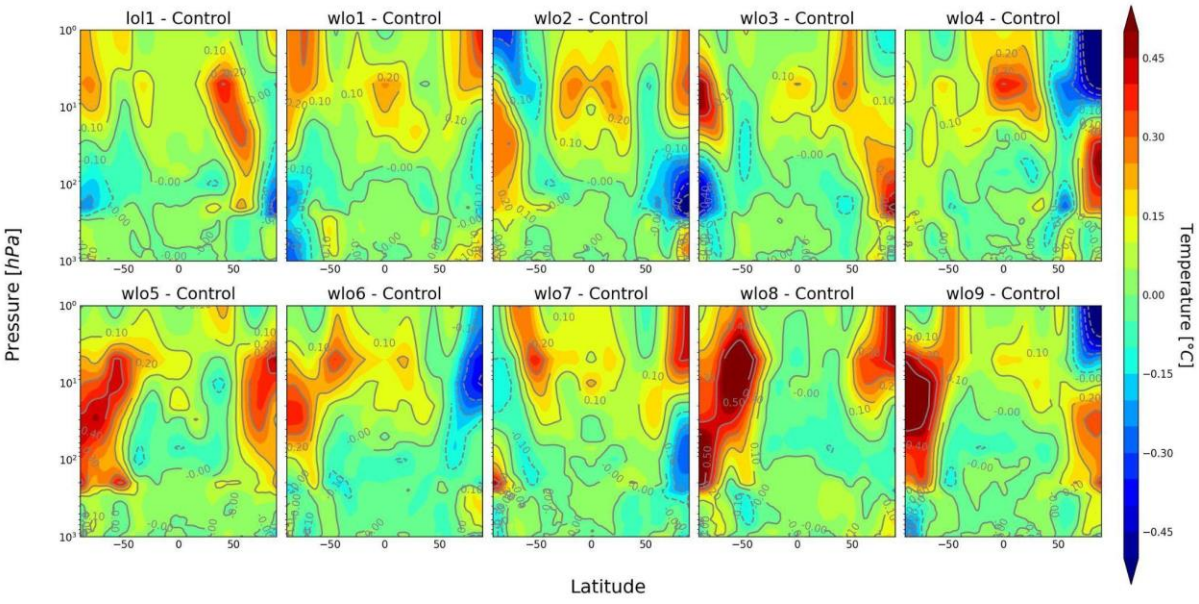

Figure 11. Time- and zonal-mean atmospheric temperature difference of each member in the WACCM ensemble with respect to the control ensemble mean.

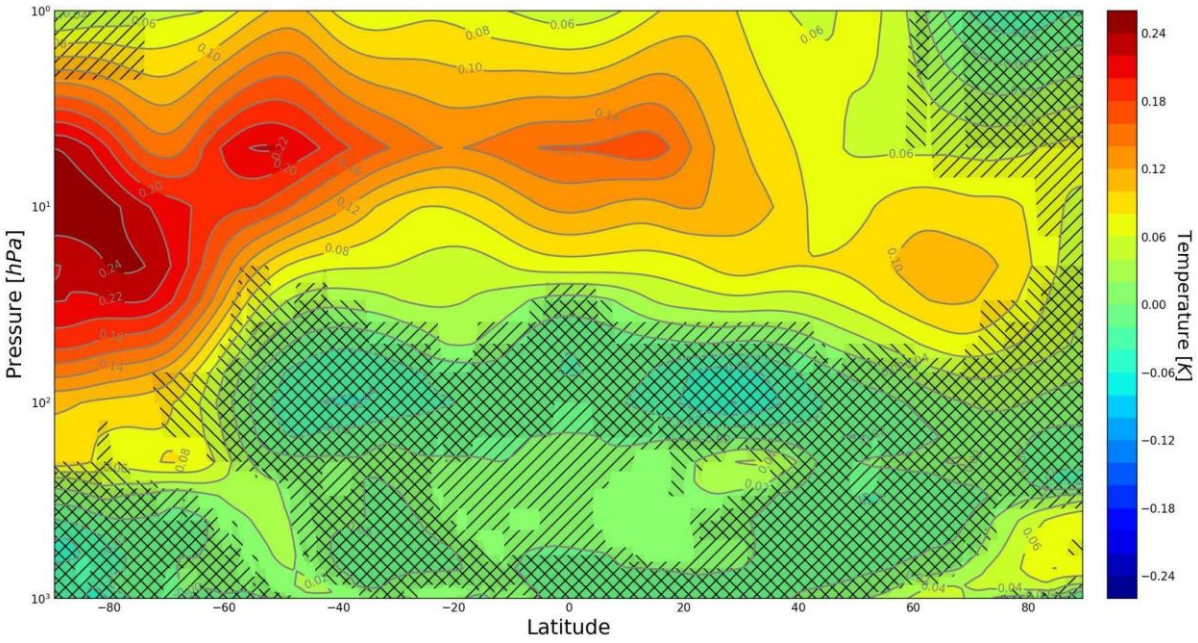

Figure 12. Time- and zonal-mean atmospheric temperature difference of the WACCM ensemble with respect to control. Slashes mask non-significant regions, i.e. where the absolute difference is smaller than the standard error of the ensemble mean; back slashes mask regions where less than eight members agree on the sign of the change.

We performed a similar ensemble analysis for the TOA (top of atmosphere) outgoing longwave radiation (OLR), considering both all-sky (including clouds) and clear-sky conditions. Figures 13 and 14 present the ensemble mean difference in OLR (all-sky and clear-sky) between the WACCM and the control ensembles. Individual members of the WACCM ensemble are also shown.

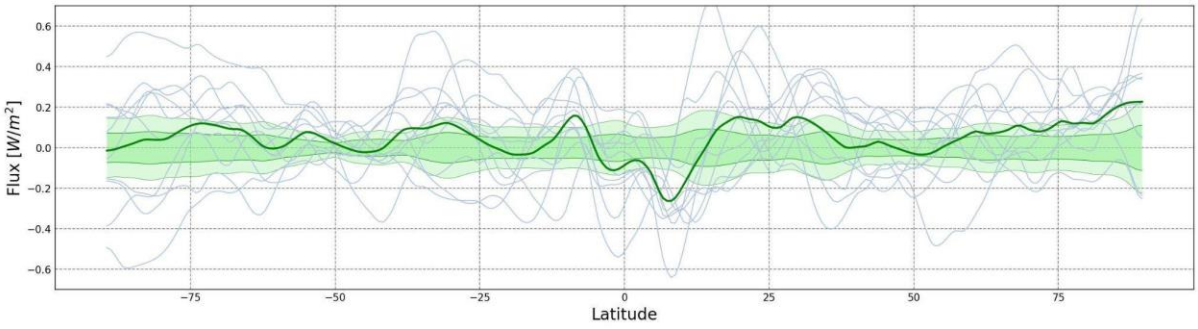

Figure 13. Difference of the time- and zonal-mean OLR of the WACCM ensemble difference with respect to the control (thick green line). Shadings show one and two mean standard errors of the ensemble control mean. Thin gray lines show individual ensemble members of the WACCM ensemble.

The average of the mean difference is positive, indicating an increased emission to space, as expected from the analysis in Section 3.1, with the exception of the Equator, where the signal is negative and appears consistent across all members. The clear sky analogue of Figure 13 is presented in Figure 14.

As expected, the variability is smaller since the signal due to clouds is removed. Here again, the mean difference is positive, while negative anomalies observed at the equator now completely disappear.

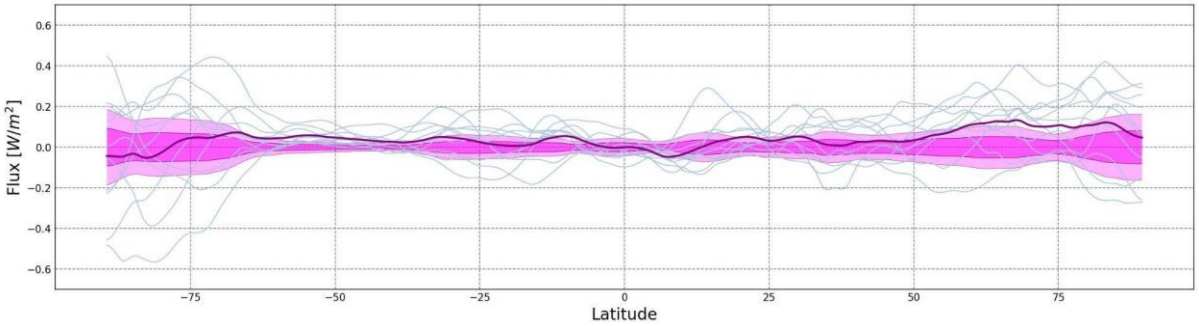

Figure 14. As Figure 13, for clear-sky fluxes.

Given the small signal, it is hard to attribute zonal changes in OLR. To better inspect the change in the OLR flux, Figures 15 and 16 show a boxplot of the global mean OLR anomaly distribution in each ensemble, computed against the control ensemble mean.

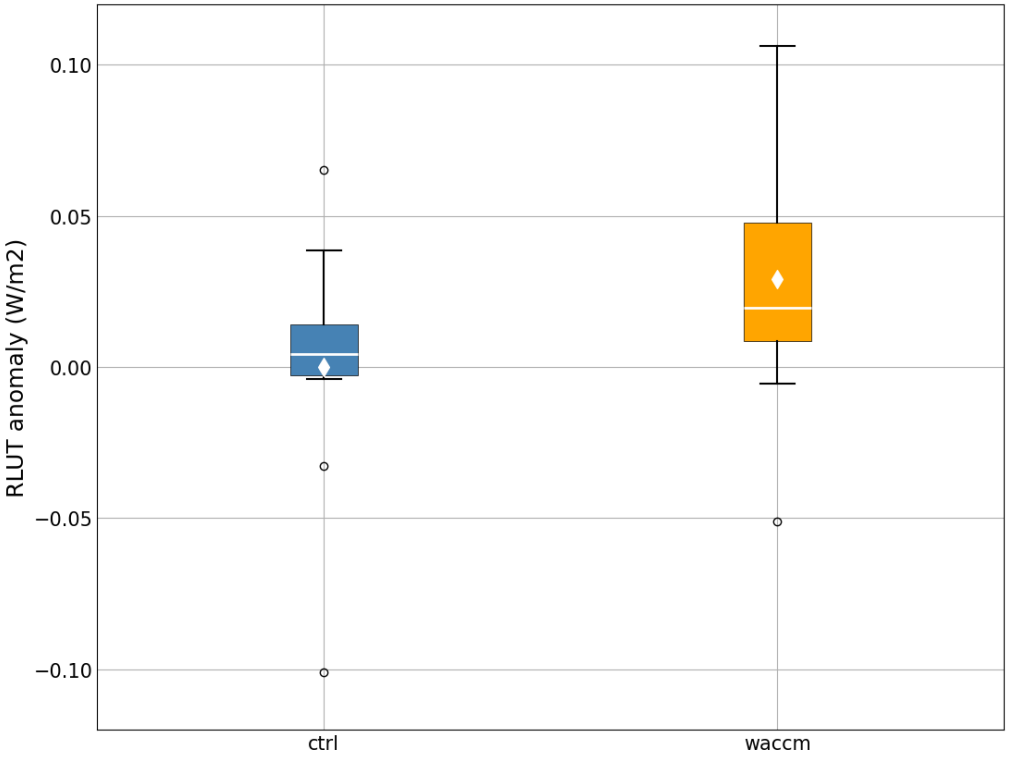

Figure 15. Boxplot of the time- and global-mean OLR anomaly distribution in each ensemble with respect to the control ensemble mean. Boxes are defined between the first and the third quantile, while the white line is the median. Whiskers show 1.5x the inter-quartile range (IQR) from the box. The diamonds show the two ensemble mean anomalies.

Figure 15 confirms the expected increase in OLR when using the modified climatology from WACCM, with a mean anomaly of about 0.03 +/- 0.02 W/m^2, which is small but significant. The signal is clearer in the clear-sky case, reported in Figure 16, which shows the two ensembles' boxes clearly separated. The mean clear-sky anomaly of the WACCM ensemble is consistent with the all-sky one, with a value of about 0.03 +/- 0.01 W/m^2.

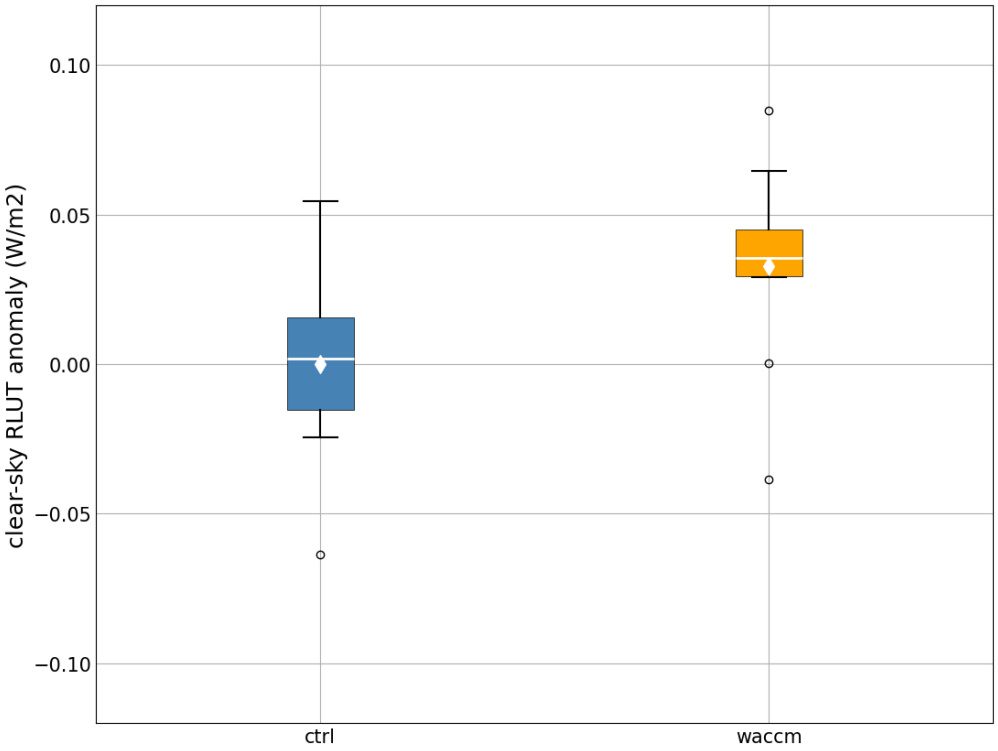

Figure 16. As Figure 15, for clear-sky fluxes

4 Conclusions and perspectives

Based on the analysis of two 10-member ensembles of atmosphere-only simulations with EC-Earth3, Section 3.2 demonstrated a statistically significant impact of the modified N_2O climatology from WACCM on the simulated climate. The results reveal a consistent warming signal in the stratosphere across almost all latitudes, with the exception of the North Pole. The warming is concentrated between 30 and 2 hPa (approximately 25-45 km altitude), spanning from the mid-stratosphere to the stratopause, with magnitudes on the order of 0.1 K. The Southern Hemisphere polar region exhibits a stronger response, with warming up to 0.3 K that extends into the lower stratosphere and upper troposphere. A clear signal has been observed also in the outgoing longwave radiation, which increased by about 0.03 +/- 0.01 W/m^2 globally in the perturbed ensemble.

The impact of the changes is small when compared to typical model temperature biases in that altitude region (which can be up to a few degrees in the stratosphere) and typical radiative biases (up to ~1W/m^2 for the global OLR). Nevertheless, the findings confirm the importance of monitoring how the vertical distribution of minor GHGs are implemented in climate models, to ensure a proper representation of the stratospheric thermal structure and its response to increased concentration.

Considering MIPAS as the best candidate to construct a new input climatology for the model (Section 2.2.2), it's worth noting that its difference with respect to WACCM is at least one order of magnitude smaller than the difference between WACCM and the original climatology used in EC-Earth3. So, the main results obtained for WACCM in Section 3.2.2 can be assumed valid also for MIPAS: assessing the difference between the latter and WACCM would require to increase by about 10 times the signal-to-noise ratio, thus requiring ~100 ensemble members, which is not computationally affordable. For this reason, the sensitivity ensemble is not repeated with MIPAS, but the main results of the analysis are expected to hold in that case as well.

An important take-away from the case study is the possibility of updating the minor GHG climatologies, starting from N_2O, as input to the EC-Earth3 model. However, some issues regarding the production of an observationally-based dataset remain to be solved. As discussed in Section 2.2.2, none of the datasets completely covers the required input range, meaning that filling of missing data and extrapolation are needed for all of them. The MIPAS dataset looks the most reliable and promising in this respect, but even in this case some parts of the monthly climatology need to be filled (in particular, in the lower stratosphere over the South pole in July). To extend the data to lower and higher altitudes, a simple constant extrapolation might be the best choice. Finally, a more philosophical issue regards the vertical scaling of the climatology applied in the model to address the change in N_2O concentration: observational datasets show a consistent increased concentration in the upper troposphere, motivated by the more recent period considered, but show a very similar concentration to WACCM in the stratosphere and above, suggesting that a uniform scaling of the column might not be the best choice to properly represent future N_2O changes.

List of acronyms and abbreviations

AGAGE	Advanced Global Atmospheric Gases Experiment
AMIP	Atmospheric Model Intercomparison Project
AOGCM	Atmosphere-Ocean General Circulation Model
CCI	Climate Change Initiative
CFC	ChloroFluoroCarbons
CMIP	Coupled Model Intercomparison Project
ECV	Essential Climate Variable
ECMWF	European Centre for Medium-Range Weather Forecasts
ERF	Effective Radiative Forcing
ESA	European Space Agency
GHG	GreenHouse Gas
GWP	Global Warming Potential
HCFC	HydroChloroFluoroCarbons
IFS	Integrated Forecasting System
IPCC	Intergovernmental Panel on Climate Change
LOLIPOP	Long Lived greenhouse gas PrOducts Performances
NOAA	National Oceanic and Atmospheric Administration
OLLGHGs	Other Long Lived GreenHouse Gases
RF	Radiative Forcing
SIC	Sea-Ice Concentration
SSPs	Shared Socio-economic Pathways

SST	Sea Surface Temperature
TOA	Top-of-the-Atmosphere
WACCM	Whole Atmosphere Community Climate Model

References

- Balsamo, G., Beljaars, A., Scipal, K., Viterbo, P., van den Hurk, B., Hirschi, M., and Betts, A. K.: A Revised Hydrology for the ECMWF Model: Verification from Field Site to Terrestrial Water Storage and Impact in the Integrated Forecast System, J. Hydrometeorol., 10, 623–643, https://doi.org/10.1175/2008JHM1068.1, 2009.

- Barath, F. T., et al., "The Upper Atmosphere Research Satellite Microwave Limb Sounder Instrument," J. Geophys. Res. 98, 10,751, 1993.

- Bernath, P. F. and McElroy, C. T. and Abrams, M. C. and Boone, C. D. and Butler, M. and Camy-Peyret, C. and Carleer, M. and Clerbaux, C. and Coheur, P.-F. and Colin, R. and DeCola, P. and DeMazière, M. and Drummond, J. R. and Dufour, D. and Evans, W. F. J. and Fast, H. and Fussen, D. and Gilbert, K. and Jennings, D. E. and Llewellyn, E. J. and Lowe, R. P. and Mahieu, E. and McConnell, J. C. and McHugh, M. and McLeod, S. D. and Michaud, R. and Midwinter, C. and Nassar, R. and Nichitiu, F. and Nowlan, C. and Rinsland, C. P. and Rochon, Y. J. and Rowlands, N. and Semeniuk, K. and Simon, P. and Skelton, R. and Sloan, J. J. and Soucy, M.-A. and Strong, K. and Tremblay, P. and Turnbull, D. and Walker, K. A. and Walkty, I. and Wardle, D. A. and Wehrle, V. and Zander, R. and Zou, J.: Atmospheric Chemistry Experiment (ACE): Mission overview, Geophys. Res. Lett., 32, L15S01, doi:10.1029/2005GL022386, 2005.

- Cariolle, D. and Brard, B.: The distribution of ozone and active stratospheric species: Result of a two-dimensional atmospheric model, in: Atmospheric Ozone, edited by: Zerefos, C. S. and Ghazi, A., pp. 77–81, D. Reidel, higham, Mass., 1984.

- Cariolle, D., and H. Teyssèdre. "A Revised Linear Ozone Photochemistry Parameterization for Use in Transport and General Circulation Models: Multi-Annual Simulations." *Atmospheric Chemistry and Physics* 7, no. 9 (May 2, 2007): 2183–96. https://doi.org/10.5194/acp-7-2183-2007.

- Döscher, Ralf, Mario Acosta, Andrea Alessandri, Peter Anthoni, Thomas Arsouze, Tommi Bergman, Raffaele Bernardello, et al. "The EC-Earth3 Earth System Model for the Coupled Model Intercomparison Project 6." *Geoscientific Model Development* 15, no. 7 (April 8, 2022): 2973–3020. https://doi.org/10.5194/gmd-15-2973-2022.

- Eyring, V., Bony, S., Meehl, G. A., Senior, C. A., Stevens, B., Stouffer, R. J., and Taylor, K. E.: Overview of the Coupled Model Intercomparison Project Phase 6 (CMIP6) experimental design and organization, Geosci. Model Dev., 9, 1937–1958, https://doi.org/10.5194/gmd-9-1937-2016, 2016

- Fichefet, T. and Maqueda, M. A. M.: Sensitivity of a Global Sea Ice Model to the Treatment of Ice Thermodynamics and Dynamics, J.Geophys. Res.-Ocean., 102, 12609–12646, https://doi.org/10.1029/97JC00480, 1997.

- Fischer, H., Birk, M., Blom, C., Carli, B., Carlotti, M., von Clarmann, T., Delbouille, L., Dudhia, A., Ehhalt, D., Endemann, M., Flaud, J. M., Gessner, R., Kleinert, A., Koopman, R., Langen, J., López-Puertas, M., Mosner, P., Nett, H., Oelhaf, H., Perron, G., Remedios, J., Ridolfi, M., Stiller, G., and Zander, R.: MIPAS: an instrument for atmospheric and climate research, Atmos. Chem. Phys., 8, 2151–2188, https://doi.org/10.5194/acp-8-2151-2008, 2008.

- Forster, Piers, Trude Storelvmo, Kyle Armour, William Collins, Jean-Luis Dufresne, David Frame, Daniel J. Lunt, et al. "Chap7 - The Earth's Energy Budget, Climate Feedbacks, and Climate Sensitivity." In *Climate Change 2021: The Physical Science Basis. Contribution of Working Group I to the Sixth Assessment Report of the Intergovernmental Panel on Climate Change*, edited by Valérie Masson-Delmotte, Panmao Zhai, Anna Pirani, Sarah L. Connors, Clotilde Péan, Sophie Berger, Nada Caud, et al., 923–1054. Cambridge, United Kingdom and New York, NY, USA: Cambridge University Press, 2021. https://doi.org/10.1017/9781009157896.001.

- U. Frisk, M. Hagström, J. Ala-Laurinaho, S. Andersson, J.-C. Berges, J.-P. Chabaud, M. Dahlgren, A. Emrich, H.-G. Florén, G. Florin, M. Fredrixon, T. Gaier, R. Haas, T. Hirvonen, Å. Hjalmarsson, B. Jakobsson, P. Jukkala, P. S. Kildal, E. Kollberg, J. Lassing, A. Lecacheux, P. Lehikoinen, A. Lehto, J. Mallat, C. Marty, D. Michet, J. Narbonne, M. Nexon, M. Olberg, A. O. H. Olofsson, G. Olofsson, A. Origné, M. Petersson, P. Piironen, R. Pons, D. Pouliquen, I. Ristorcelli, C. Rosolen, G. Rouaix, A. V. Räisänen, G. Serra, F. Sjöberg, L. Stenmark, S. Torchinsky, J. Tuovinen, C. Ullberg, E. Vinterhav, N. Wadefalk, H. Zirath, P. Zimmermann, R. Zimmermann: The Odin satellite - I. Radiometer design and test, A&A 402 (3) L27-L34, DOI: 10.1051/0004-6361:20030335, 2003.

- Hassan MU, Aamer M, Mahmood A, Awan MI, Barbanti L, Seleiman MF, Bakhsh G, Alkharabsheh HM, Babur E, Shao J, Rasheed A, Huang G. "Management Strategies to Mitigate N2O Emissions in Agriculture". Life (Basel). 2022 Mar 17;12(3):439. doi: https://doi.org/10.3390/life12030439

- Hogan, Robin J., and Alessio Bozzo. "A Flexible and Efficient Radiation Scheme for the ECMWF Model." *Journal of Advances in Modeling Earth Systems* 10, no. 8 (2018): 1990–2008. https://doi.org/10.1029/2018MS001364.

- Madec, G., Bourdallé-Badie, R., Bouttier, P.-A., et al.: NEMO ocean engine, In Notes du Pôle de modélisation de l'Institut Pierre-Simon Laplace (IPSL) (v3.6-patch, Number 27), Zenodo, https://doi.org/10.5281/zenodo.3248739, 2017.

- Meinshausen, Malte, Elisabeth Vogel, Alexander Nauels, Katja Lorbacher, Nicolai Meinshausen, David M. Etheridge, Paul J. Fraser, et al. “Historical Greenhouse Gas Concentrations for Climate Modelling (CMIP6).” *Geoscientific Model Development* 10, no. 5 (May 31, 2017): 2057–2116. https://doi.org/10.5194/gmd-10-2057-2017.

- O’Neill, B. C., Tebaldi, C., van Vuuren, D. P., Eyring, V., Friedlingstein, P., Hurtt, G., Knutti, R., Kriegler, E., Lamarque, J.-F., Lowe, J., Meehl, G. A., Moss, R., Riahi, K., and Sanderson, B. M.: The Scenario Model Intercomparison Project (ScenarioMIP) for CMIP6, Geosci. Model Dev., 9, 3461–3482, https://doi.org/10.5194/gmd-9-3461-2016, 2016.

- Waters, J.W., W.G. Read, L. Froidevaux, R.F. Jarnot, R.E. Cofield, D.A. Flower, G.K. Lau, H.M. Pickett, M.L. Santee, D.L. Wu, M.A. Boyles, J.R. Burke, R.R. Lay, M.S. Loo, N.J. Livesey, T.A. Lungu, G.L. Manney, L.L. Nakamura, V.S. Perun, B.P. Ridenoure, Z. Shippony, P.H. Siegel, R.P. Thurstans, R.S. Harwood, H.C. Pumphrey, M.J. Filipiak, “The UARS and EOS Microwave Limb Sounder Experiments,” J. Atmos. Sci. 56, 194-218, 1999.

***** End of Document *****